# Extending the reach of FWI with reflection data: Potential and challenges

*Adriano Gomes* and Nicolas Chazalnoel, CGG*

**Summary**

We present a Reflection FWI (RFWI) workflow to update the velocity model using the low-wavenumber component of the FWI gradient of reflection data. This is achieved by alternately using high-wavenumber and low-wavenumber components to update density and velocity models, respectively. With synthetic examples, we discuss the limitations and requirements of this approach and propose possible ways to overcome some of the limitations. Finally, the method is applied to a deep-water survey in the Gulf of Mexico, where improvement is observed both in the migrated image and gathers.

**Introduction**

Despite the increasing popularity of full waveform inversion (FWI) (Tarantola, 1984), the improvements it makes to the velocity model and seismic image are often insufficient to fully resolve the complexity in deeper areas. This is due to the well-known depth limitation of the diving waves that are normally used to drive FWI (Sirgue and Pratt, 2004), being caused by practical constraints on the maximum offset recorded in the seismic data and the local velocity regime, as well as the low signal-to-noise ratio of the diving-wave low-frequency energy at large offsets (Dellinger et al., 2017).

One option to address this limitation is to look to reflection data, which contain information about deeper events. However, the modeling of reflection data requires a reasonably accurate velocity model and density/reflectivity model in order to avoid cycle-skipping at higher frequencies (Virieux and Operto, 2009) and to model the correct relative amplitudes (Guitton, 2014). When these conditions are met, reflection data can be used in standard FWI to add detailed features to the velocity model (Qin et al., 2014). However, the high vertical-wavenumber component that dominates the FWI gradient of reflection data has limited impact on the model kinematics.

In the last few years, several methods have been proposed to increase the significance of reflection data in the FWI workflow, e.g., Xu et al. (2012), Tang et al. (2013), Brossier et al. (2014), Alkhalifah et al. (2014), Irabor and Warner (2016), Vigh et al. (2016), and Ramos-Martinez et al. (2016), among others. A common feature in all these methods is the extraction and/or enhancement of the low-wavenumber component of the FWI gradient of reflection data. As shown by Mora (1989), reflection data produce two different components in the FWI gradient: the high-wavenumber component, also known as the migration term, and the low-wavenumber component, also known as the tomographic term or "rabbit ears" (Figure 1). This tomographic term is generated along the reflection wavepath; therefore, it contains significant information about the kinematics of the velocity model, including areas beyond the reach of diving waves.

In this paper, an RFWI method to update the velocity model using the rabbit ears is presented. Based on synthetic tests, the limitations and requirements of this approach are discussed. Finally, the method is applied to a deep-water survey in the Gulf of Mexico.

**Method**

In practice, using the rabbit ears in RFWI has two basic conditions: it requires some model or gradient decomposition to decouple the influence of the migration term from that of the tomographic term, and it requires sharp boundaries in the model to generate the backscattered energy that will form the rabbit ears.

The terms of the gradient can be distinguished by the direction of propagation of the source and residual wavefields (Mora, 1989). The separation can be achieved by explicit model separation using the Born approximation (Xu et al., 2012; Vigh et al., 2016) or by decomposition techniques, such as inverse-scattering imaging condition (Ramos-Martinez et al., 2016), scattering-angle filter (Alkhalifah et al., 2014), or wavefield decomposition (Tang et al., 2013; Irabor and Warner, 2016).

In our work, an up-down wavefield decomposition method proposed by Liu et al. (2011) is used to separate the components of the gradient:

$$g_t(\mathbf{x}) = \frac{1}{2}\int_0^{t_{max}} s(\mathbf{x},t)r(\mathbf{x},t) + H_z(s(\mathbf{x},t))H_z(r(\mathbf{x},t))dt$$
$$g_m(\mathbf{x}) = \frac{1}{2}\int_0^{t_{max}} s(\mathbf{x},t)r(\mathbf{x},t) - H_z(s(\mathbf{x},t))H_z(r(\mathbf{x},t))dt \quad , \quad (1)$$

where $s$ is the source wavefield, $r$ is the back-propagated residual wavefield, $H_z$ represents the Hilbert transform in $k_z$ direction, and $g_t$ and $g_m$ are the tomographic and migration terms, respectively.

In order to produce the back-scattered energy necessary to generate the rabbit ears, a bootstrapping approach is used to estimate the location of the reflectors. More specifically, in the first iteration, the high-wavenumber component $g_m$ of

the gradient is used to estimate a density model that will contain the necessary sharp contrasts. This is followed by a velocity update iteration, this time using the low-wavenumber component $g_t$ of the gradient. These iterations are then alternated, meaning that both the background velocity and reflector locations are sequentially updated, until a convergence criterion is reached.

Although the assumption that all reflection data are generated by density contrasts is not precise, the placement of the reflectors is consistent with the current velocity model; therefore, the traveltime information obtained with the estimated density model can be used to infer kinematic errors in the background velocity model.

In the proposed method, the least-squares objective function (Tarantola, 1984) is chosen as the misfit measurement between real and modeled data, though different objective functions can be used within the general RFWI framework (Brossier et al., 2014; Vigh et al., 2016).

**Simple synthetic example**

A simple two-layer model, consisting of a constant velocity of 2000 m/s with a density contrast at $z$ = 3000 m, is used to illustrate the RFWI operation. In this test, two different initial models are compared, one with 5% lower velocity and another with 5% higher velocity. In both cases, an initial constant density model is provided to RFWI. The maximum offset in the data is 4000 m, and a maximum frequency of 10 Hz is used for the RFWI iterations.

For these tests, zero-offset data are used to update the density model at the first iteration, using the high-wavenumber component of the gradient. This is followed by a velocity update iteration. Because the reflector depth is self-derived from each initial model, both tests match the observed data at zero-offset. RFWI will then derive the velocity update from the data mismatch at different offsets. In practice, any offset group can be used as the reference to estimate the reflector location at the first iteration, although that does not guarantee convergence to the same final model, since some offsets might have large accumulated errors, increasing the chance of convergence to local minima if used as the reference. If all offsets are used in the first iteration, the stacked migration term is typically dominated by the near offset data. However, for complex geologies, the curvature of migrated gathers can take more complicated shapes.

Figures 1a and 1b show the RFWI low-wavenumber velocity update using a single trace with 3000 m offset. Figures 1c and 1d show the update for 700 shots. The derived density model in the first iteration is shown in the background. In both cases, the correct update direction is obtained, i.e., speed up (red) for the 5% slower model and slow down (blue) for the 5% faster model. Nonetheless, it is important to note that, although the reflector location is self-derived from the velocity model, RFWI is still susceptible to cycle-skipping, as the timing error normally increases as we go further from the reference offset.

It is clear that despite having the potential to extend the maximum update depth beyond that of diving-wave FWI, RFWI is also subject to its own restrictions, due to the "tomographic" nature of the problem. In the following two sections, some limitations of this approach are revisited, focusing on the contribution provided by deeper layers.

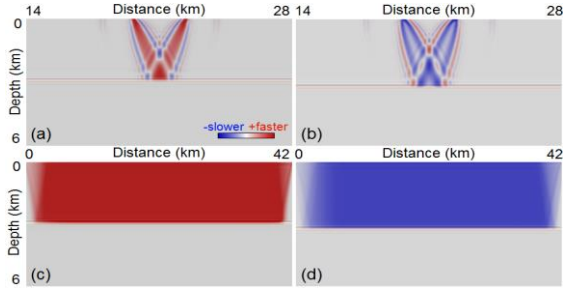


**Figure 1:** RFWI update using: (a) and (c) 5% slower model; (b) and (d) 5% faster model. The top row corresponds to the gradient of a single shot, with a single offset of 3000 m. The bottom row corresponsts to the gradient of all shots and offsets.

**Resolution analysis**

First, we analyze the wavenumber resolution of the RFWI gradient. For this purpose, we use the model shown in Figure 2, which contains three velocity anomalies with different wavenumber contents. The density model contains a single reflector at $z$ = 10 km, indicated by the black line. From this model, we created a data set with maximum offset of 8 km and maximum frequency of 20 Hz.

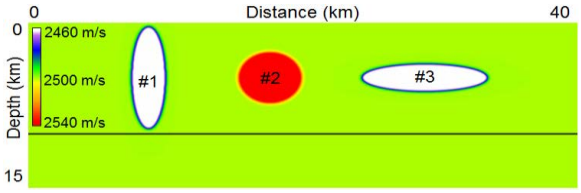


**Figure 2:** (a) Velociy model with three different shaped anomalies.

Taking these parameters into account, the wavenumber resolution of the RFWI gradient — i.e., the model wavenumbers that are sampled by RFWI — is analytically calculated as in Zhou (2016) and shown in Figure 3. As previously stated, the RFWI gradient is formed along the reflection wavepath, i.e., by crosscorrelation of the scattered source wavefield and incident receiver wavefield (and vice-versa). As the reflector gets deeper, the reflection angle normally decreases, given the offset limitation in the recorded data set. Therefore, for mildly dipping events, the reflection wavepath becomes more vertical, which means that rapid horizontal variations can be naturally sampled by different scattering points along the reflector. However, rapid vertical variations are averaged out along the wavepath. This effect can be observed in Figure 3, in which

the RFWI gradient (in red) provides good coverage of the horizontal wavenumbers ($k_x$), but it is concentrated around the low vertical wavenumbers ($k_z$).

In addition to the RFWI gradient, the dominant wavenumbers (larger than -30 dB) of each anomaly in Figure 2 are calculated and plotted in Figure 3. Comparing the spectra, it is clear that Anomaly #1 is well aligned with the RFWI gradient, while the other two have many wavenumbers that are not sampled by the deep reflector.

Figure 4 shows the RFWI result, starting from a constant velocity of 2500 m/s, after a total of 35 iterations. As expected from the wavenumber analysis, while horizontal wavenumbers are well resolved, only the small vertical wavenumbers are recovered by RFWI. This is sufficient for Anomaly #1 but insufficient for Anomalies #2 and #3, which contain higher vertical wavenumbers. As a result, Anomaly #1 is well resolved and the other two are smeared vertically from the reflector location to the surface. However, a migration QC indicates that, for all three anomalies, the kinematics of the velocity model are well recovered at the reflector depth.

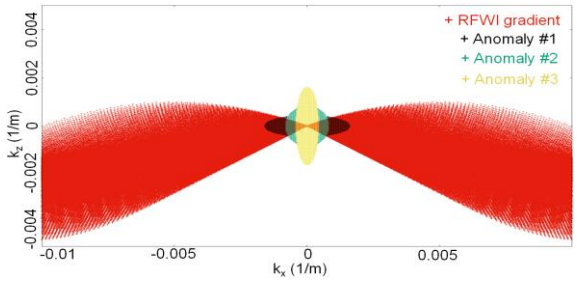


**Figure 3:** Wavenumber spectrum of RFWI gradient overlaid with spectra of velocity anomalies.

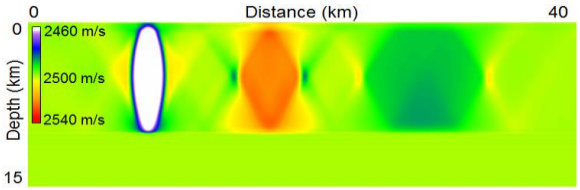


**Figure 4:** RFWI result after 35 iterations.

In practice, the spectrum of the RFWI gradient can be extended by the presence of additional reflectors at different depths and with varying dips (Alkhalifah, 2016). However, unlike tomographic methods based on residual moveout, in which each sensitivity kernel — i.e., the sensitivity of the data residual to the model parameters — is computed individually, the contribution of many kernels is calculated simultaneously in RFWI. As a result, the sensitivity kernel is more susceptible to the effects of amplitude imbalance, such as poor illumination or low reflectivity events. Ultimately, this can lead to an initial dominance by stronger events, which can introduce a bias towards certain wavenumbers. To alleviate this problem, strategies such as top-down inversion and regularization can be considered.

**Reflector depth uncertainty**

Another challenge faced by RFWI is the uncertainty regarding the true reflector depth. Unlike conventional diving-wave FWI, which only requires a smooth velocity, RFWI needs sharp contrasts in the model in order to generate the backscattered energy that forms the rabbit ears. Since the traveltimes depend on both velocity and reflector position, the non-linearity of the problem is increased, i.e., RFWI can converge to incorrect velocities and reflector depths that still match the traveltimes, just as ray-based reflection tomography can.

This problem is illustrated in Figure 5, in which RFWI using only deep reflectors is performed with (Figure 5c) and without (Figure 5d) a priori information about the reflector depths. Since the initial velocity error is large (up to 30%) and there are not enough events to fully constrain the inversion, RFWI without a priori information converges to an alternative model that does not give the correct stacked image, although it improves the flatness of the migrated gathers (Figure 5h). On the other hand, with a priori information about the reflector depth, RFWI correctly recovers the wavenumbers sampled by the deep reflector and is able to match the true image (Figure 5b) at that depth.

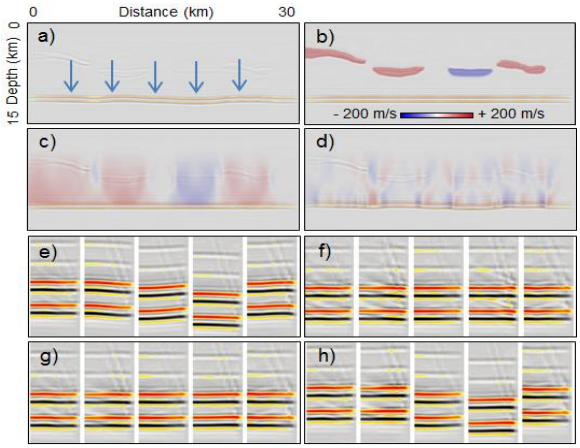


**Figure 5:** Migrated image and velocity perturbation: a) Initial, b) true model, c) RFWI with a priori information, d) RFWI without a priori information. e), f), g), and h) are SOGs corresponding to models a), b), c), and d) respectively. The location of the gathers is indicated by the arrows.

Although this velocity-depth ambiguity is well known in migration velocity analysis (MVA) methods (Stork, 1992), imposing constraints in RFWI is less straightforward since the contribution from many events is combined together. Therefore, for the moment, we recommend applying RFWI starting from a reasonably good initial model, in which the location and focusing of the reflectors are not too damaged.

## Real data example

Finally, we applied RFWI to a deep-water survey on the Mexican side of the Gulf of Mexico (GoM). The area of interest is located on the prolific Perdido fold belt. The water bottom depth ranges from 200 m to 3500 m. The seismic data were acquired using a flat-cable wide-azimuth (WAZ) acquisition configuration with maximum offset of 8.1 km along the cables and 4.2 km across the cables.

The initial model for RFWI (Figure 6a) was obtained after diving-wave FWI, along with velocity scans and ray-based tomography for the deeper shales (Chazalnoel et al., 2017). However, due to the complexity of the folds combined with the low reflectivity of the shales in the overburden, some discontinuities remain at the deep Wilcox and Cretaceous events (white arrows in Figure 6a). These discontinuities can also be observed on the gathers (Figure 6d).

RFWI was then performed from 4 to 7 Hz, using data after source and receiver deghosting, zero-phasing, and SRME demultiple. After RFWI application, a significant improvement is observed in the continuity of deeper events, both in the migrated image and gathers (Figures 6b and 6e).

An analysis of the RFWI perturbation (Figure 6c) reveals more consistency with the structures in the fold area, while the perturbation in the deeper part consists mostly of low vertical wavenumbers. This is due to stronger contributions from the deep events around 10 km, compared with the low reflectivity shales between the shallow folds and the deep events. However, the recovered wavenumbers are still able to significantly improve the kinematics throughout the section, most notably at the Wilcox and Cretaceous but also in the shales, and the final velocity model has good consistency with the geology.

## Discussion and conclusions

We have shown that RFWI has the potential to extend low-wavenumber updates of FWI to much deeper areas, beyond the reach of diving waves. In fact, RFWI shares many concepts with MVA methods, such as ray-based reflection tomography. However, since the contributions from many events are calculated simultaneously, RFWI is susceptible to the effects of amplitude imbalance, which can lead to limited vertical resolution and convergence to local minima. Therefore, at the current stage, RFWI can be viewed as a complement, rather than a replacement, to established velocity inversion methods. Nonetheless, the significant improvement obtained by RFWI in the real data example shows that this technique is worth understanding and improving further, as it could become a valuable tool for updating the deeper section of velocity models.

## Acknowledgments

We thank CGG Multi-Client & New Ventures and the Mexican Comisión Nacional de Hidrocarburos for permission to show these results.

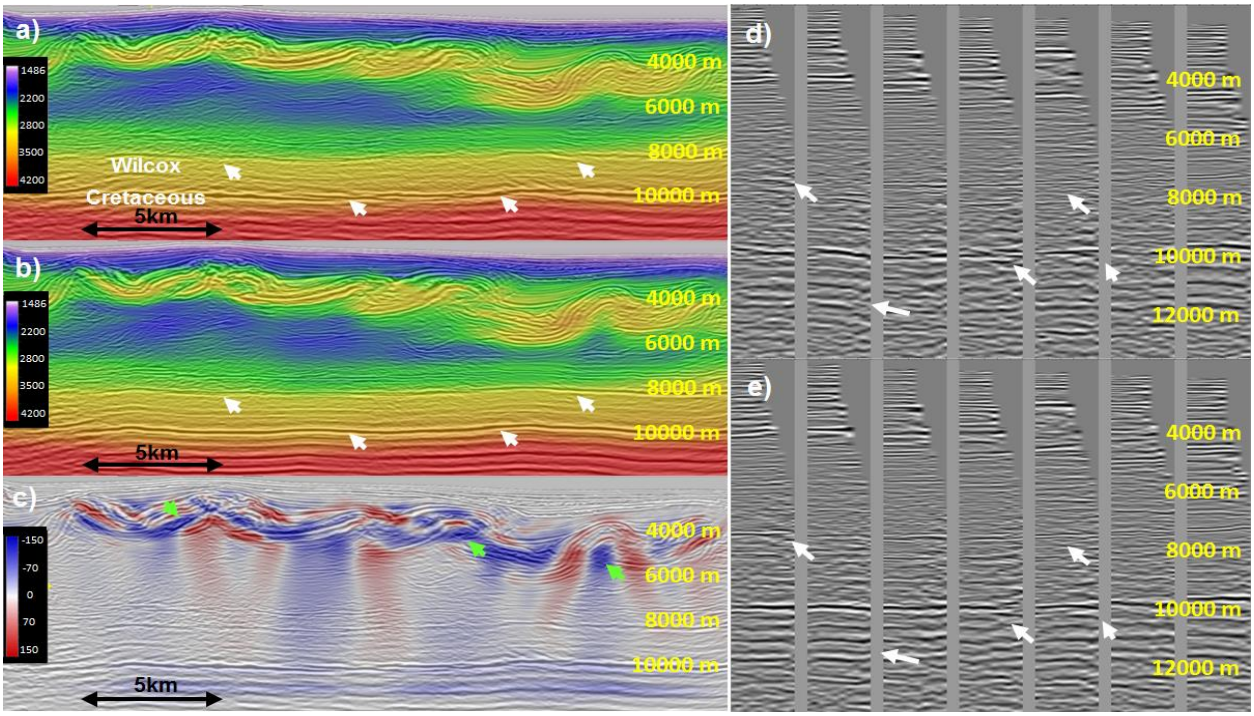


**Figure 6:** Vertical section with the velocity model overlaid on an RTM stack for: a) initial model, b) RFWI updated model, and c) RFWI velocity perturbation. RTM surface offset gathers over the same line from: d) initial model, and e) RFWI updated model.